DALTON
PERSPECTIVE

Oxygen activation at non-heme diiron active sites in biology: lessons from model complexes*

Lawrence Que, Jr.

Department of Chemistry and Center for Metals in Biocatalysis, University of Minnesota, Minneapolis, Minnesota 55455, USA

In the past few years a number of iron complexes have been synthesized and characterized that model features of intermediates involved in the oxygen-activation chemistry of non-heme diiron enzymes such as methane monooxygenase, ribonucleotide reductase, and fatty acid desaturases. Insights derived from these efforts are discussed in the context of a common mechanistic framework for these enzymes.

Carboxylate-bridged non-heme diiron active sites have emerged in the past decade as a new common structural motif for an increasing number of metalloproteins that bind and/or activate dioxygen.[1] The proteins belonging to this class include: the invertebrate respiratory protein hemerythrin (Hr),[2] the R2 protein of ribonucleotide reductase (RNR R2), a key enzyme in DNA biosynthesis,[3] the hydroxylase component of methane monooxygenase (MMOH) found in methanotrophic bacteria[4] and fatty acid desaturases, which convert saturated fatty acids into their unsaturated derivatives in plant metabolism.[5] The range of dioxygen-dependent reactions carried out by this non-heme diiron active site now appears to rival in versatility those that occur at heme active sites.[6]

X-Ray crystallography has contributed significantly to our understanding of the bioinorganic chemistry of these non-heme diiron metalloproteins; the crystal structure of at least one form of each of the proteins mentioned above has been solved.[2–5] Shown on the left column of Fig. 1 are structures representing the diiron(II) forms of each protein. In each structure the diiron(II) unit is bridged by two carboxylate groups, all co-ordinating in a bidentate fashion except in MMOH where one carboxylate acts as a monodentate bridge; there is also an additional hydroxo bridge present in deoxyhemerythrin. These variations in the bridges that hold the diiron(II) unit together rationalize the range of Fe · · · Fe distances found in these structures: 3.3 Å for Hr[2] and MMOH,[4b] 3.9 Å for RNR R2,[3b] and 4.2 Å for stearoyl-ACP Δ^9-desaturase (Δ9D).[5]

It is interesting that hemerythrin, originally considered to be the prototype of this class, turns out to be the most distinct from the other three in several respects.[2] First of all, deoxyhemerythrin is the only one with a triply bridged diiron(II) cluster. Secondly, Hr has five terminal histidine (His) ligands, a ligand combination not found in the other three proteins. Lastly, deoxyhemerythrin has only one co-ordination site available for exogenous ligands, to which O_2 binds, as shown by the crystal structure of oxyhemerythrin[2] (Fig. 1). Upon dioxygen binding the (μ-hydroxo)bis(μ-carboxylato)diiron(II) core is converted into a (μ-oxo)bis(μ-carboxylato)diiron(III) core, and O_2 is reduced to a terminal hydroperoxide that is hydrogen bonded to the oxo bridge.[8] Thus two electrons and the μ-hydroxo proton are transferred to the O_2 upon binding. As befits the reversible nature of dioxygen binding in this protein, there is minimal change in the co-ordination environments of the metal centres in the deoxy and oxy forms.

The other three active sites show a remarkable similarity despite their different functions. Besides all having a bis(μ-carboxylato)diiron(II) core, all three have two His and two carboxylate residues as terminal ligands. Furthermore each His residue is separated from one of the carboxylate ligands by two residues. This pair of (Asp/Glu)-X-X-His sequence motifs[7] is now being used as an indicator that such a non-heme diiron active site may be found in enzymes such as phenol hydroxylase and toluene monooxygenases.[9] Indeed Δ9D was first suggested to have a non-heme diiron active site on this basis, which was subsequently confirmed by spectroscopic studies[7b,10] and X-ray crystallography.[5] More importantly, the iron(II) centres of all three enzymes are four- or five-co-ordinate, thus allowing each iron to participate in dioxygen binding and activation. Unlike the case of Hr, there are significant changes in the co-ordination environments of MMOH and RNR R2 upon oxidation to their diiron(II) forms[3,4] (no crystallographic data available

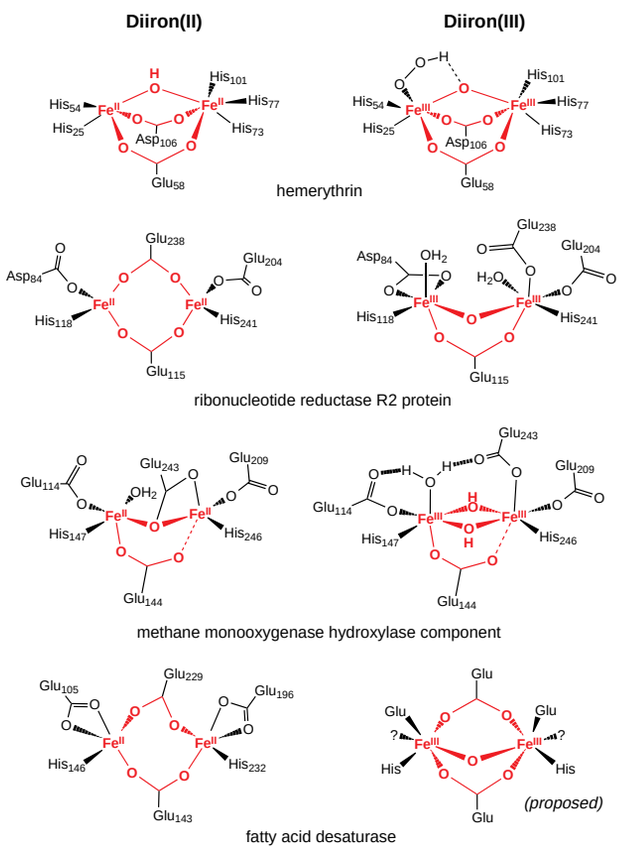

Fig. 1 Non-heme diiron active sites of hemerythrin, ribonucleotide reductase R2 protein, the hydroxylase component of methane monooxygenase, and stearoyl Δ^9-ACP desaturase as determined by X-ray crystallography (from refs. 2–5). The structure proposed for the oxidized desaturase is adapted from ref. 7(*b*)

* Based on the presentation given at Dalton Discussion No. 2, 2nd–5th September 1997, University of East Anglia, UK.

Table 1 Properties of diiron(III)–peroxo species

Complex	r(Fe–O_{peroxo})/Å	$\tilde{\nu}$(O–O)($\Delta^{18}O_2$)/cm^{-1}	δ/mm s^{-1}	Ref.
Oxyhemerythrin		844 (−47)	0.51, 0.52	17
MMOH-**P**		905 (−25)	0.66	16
$[Fe_2(\mu\text{-}O_2)L^1(\mu\text{-}O_2CCH_2Ph)_2]$	1.876(6), 1.877(6), 1.881(6), 1.905(6)	888 (−46)	0.66	22
$[Fe_2(\mu\text{-}O_2)L^2(OPPh_3)_2]^{3+}$	1.880(4)	900 (−50)		21
$[Fe_2(\mu\text{-}O_2)L^2(O_2CPh)]^{2+}$		900 (−50)	0.52	18
$[Fe_2(\mu\text{-}O_2)L^3(O_2CPh)]^{2+}$	1.864(4), 1.944(4)	not observed	0.58, 0.65	20
$[Fe_2(\mu\text{-}O_2)L(O_2CPh)]^{2+}$ [a]		918, 891 (−43)		19(*b*)
$[Fe_2(\mu\text{-}O_2)L(O_2CPh)]^{2+}$ [b]		893, 877 (−51)		18(*b*)

[a] R = R′ = Me. [b] R = R′ = H.

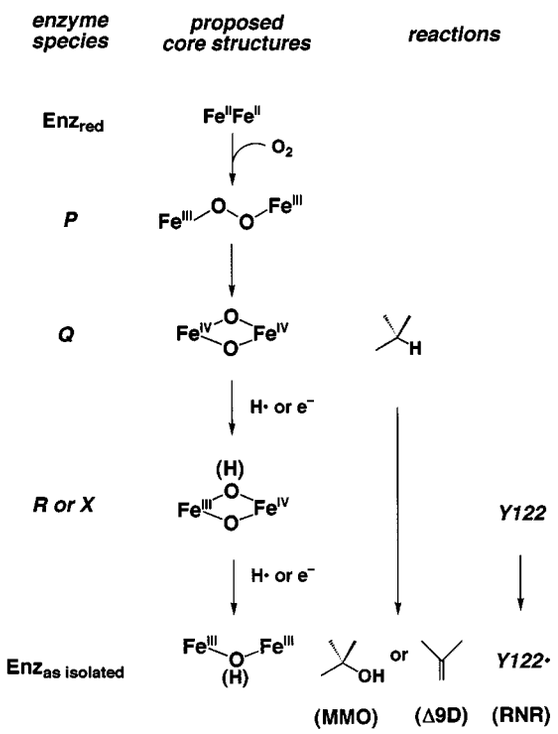

Scheme 1 Proposed common mechanism for oxygen activation by diiron centers in non-heme diiron enzymes

for Δ9D). In particular, one of the bridging carboxylates undergoes a 'carboxylate shift'[11] to become a terminal ligand in the diiron(III) forms (Fig. 1, right column).

The structural similarities among the diiron sites of MMOH, Δ9D, and RNR R2 have led us[12] and others[1b,13] to propose a common mechanism for oxygen activation to carry out the respective oxidative functions of the three enzymes (Scheme 1). This mechanism consists of: (i) the initial interaction of O_2 with the diiron(II) center affording a diiron(III) peroxide species; (ii) the subsequent cleavage of the peroxide O–O bond to form a diiron(IV) species and (iii) the reduction of this high-valent species *via* a diiron(III,IV) intermediate to afford the as-isolated diiron(III) state. It should be noted that the structures proposed in the mechanistic scheme for the various intermediates merely serve to illustrate some of the structures that can represent a particular oxidation state, and there are other possible alternative formulations.

Support for this scheme has accumulated in recent years from rapid kinetic studies of the reaction of O_2 with the diiron(II) forms of RNR R2[14] and MMO[15,16] in which kinetically competent catalytic intermediates have been observed and characterized spectroscopically. The observation of such species in the enzyme reactions has in turn stimulated efforts to generate and characterize analogous intermediates in model systems to serve as synthetic inorganic precedents for the chemistry of these non-heme diiron enzymes.

Dioxygen Binding to a Diiron(II) Center

The binding of O_2 to Hr is a reversible process in which two electrons from the diiron(II) unit are transferred to O_2 to form a diiron(III) center with a terminal hydroperoxide (Fig. 1). This description for oxyhemerythrin is supported by the appearance of a visible band (λ_{max} 500 nm) attributed to a peroxo-to-iron(III) charge-transfer transition and confirmed by a ν(O–O) feature at 844 cm^{-1} in its resonance-Raman spectrum[8] (Table 1). Consistent with the presence of two distinct iron coordination environments in the crystal structure of oxyhemerythrin, two Mössbauer doublets are observed ($\delta = 0.51$ and 0.52 mm s^{-1}, $\Delta E_Q = 1.96$ and 0.95 mm s^{-1}) with isomer shifts typical of high-spin iron(III) ions.[17]

Similarly, the reaction of O_2 with $MMOH_{red}$ affords intermediate **P**,[15a,16] which is also described as a diiron(III)–peroxide species on the basis of its spectroscopic properties (Table 1).[16] The species MMOH-**P** exhibits a visible absorption maximum in the 600–700 nm region associated with a peroxo-to-iron(III) charge-transfer transition and an oxygen-isotope-sensitive Raman band near 905 cm^{-1} arising from the bound peroxide. In contrast to oxyhemerythrin, MMOH-**P** exhibits only one Mössbauer doublet ($\delta = 0.66$ mm s^{-1}, $\Delta E_Q = 1.51$ mm s^{-1}), indicating similar iron sites, with an isomer shift that is somewhat higher than is typical for high-spin Fe^{III}. There are also some preliminary data suggesting that a **P**-like species forms in the reaction of RNR $R2_{red}$ with O_2 [footnote 12 in ref. 14(*e*)], supporting the notion that the carboxylate-rich diiron active sites utilize a common mechanism for activating O_2.

Designing synthetic non-heme iron(II) complexes that can bind O_2 to model oxyhemerythrin and MMOH-**P** has been a goal of a number of research groups, and several systems have been developed in the past few years.[18,19,23] These efforts culminated with the first crystal structures of synthetic diiron(III) peroxide complexes, which were reported in rapid succession in 1996[20–22] and are illustrated in Fig. 2.

Kitajima *et al.*[23a] reported in 1990 the use of ligand L^1 to form a five-co-ordinate $[Fe^{II}L^1(O_2CR)]$ complex that reversibly bound O_2 at −20 °C in toluene (R = Me or Ph). On the basis of spectroscopic studies, the dioxygen adduct was proposed to be a (μ-1,2-peroxo)diiron(III) species (Table 1). The crystal structure of the phenylacetate derivative subsequently solved by Kim and Lippard[20] shows such a peroxo-bridged diiron species supported by bridging carboxylates.

Que and co-workers[18a] also reported in 1990 the use of a dinucleating ligand with a 1,3-diamino-2-hydroxypropane backbone and pendant benzimidazoles to afford a diiron(II) complex $[Fe_2L^2(O_2CPh)][BF_4]_2$ with trigonal-bipyramidal iron centers. This complex binds O_2 quantitatively in CH_2Cl_2 or MeCN to afford an irreversible adduct at −40 °C, proposed on the basis of spectroscopic evidence (Table 1) to have a (μ-1,2-peroxo)(μ-alkoxo)(μ-benzoato)diiron(III) core. Interestingly, its lifetime of a few hours at −40 °C in MeCN could be extended to weeks by the addition of 50 equivalents Ph_3PO, which allowed diffraction-quality crystals to be grown. The structure

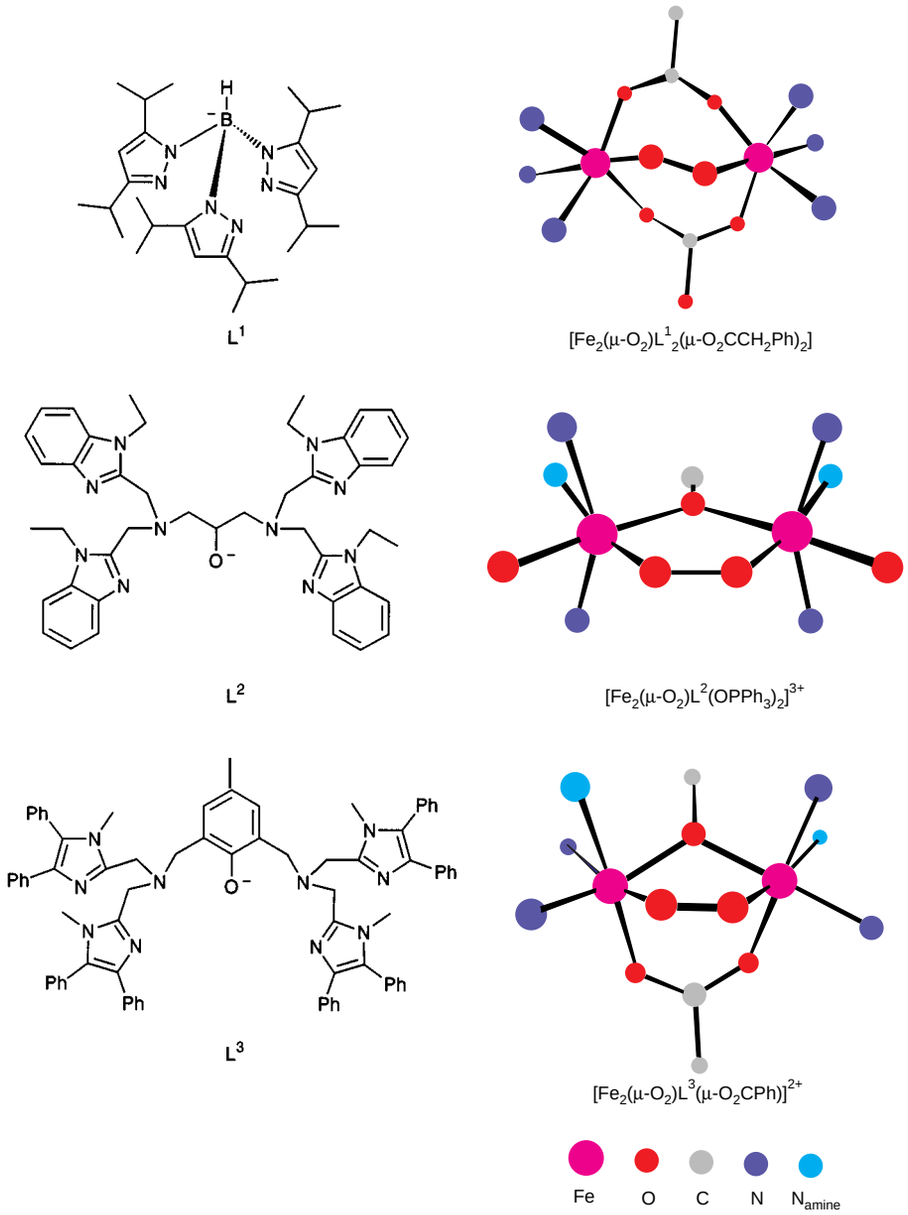

Fig. 2 Structures of synthetic dioxygen adducts from refs. 20–22

showed the expected alkoxo and 1,2-peroxo bridges, but the bridging benzoate had been displaced by phosphine oxides.[21]

Suzuki and co-workers[19] also worked on dinucleating ligands with a 2-hydroxypropane backbone and obtained a reversible dioxygen adduct by suitable manipulation of the terminal ligands. Subsequently, they designed another dinucleating ligand L^3 which provides a phenolate to act as a bridge between iron centers and pendant imidazoles with bulky phenyl substituents as terminal ligands. The diiron(II) complex of this ligand also binds O_2 reversibly and the crystal structure revealed an adduct with a (μ-1,2-peroxo)(μ-phenoxo)(μ-benzoato)diiron(III) core;[22] indeed this structure represents the first of the three reported in 1996.

The three structures reveal a number of interesting features for these dioxygen adducts (Fig. 2, Table 1). In all three cases, the dioxygen adducts derive from co-ordinatively unsaturated iron(II) precursors. The O–O bond lengths are 1.42 ± 0.01 Å, in agreement with the peroxide formulation for the 1,2-dioxygen bridge. The Fe^{III}–O_{peroxo} bond lengths average 1.88 Å, comparable to Fe^{III}–OH bond lengths[24] and consistent with the basicity of the peroxide ligand. The peroxide co-ordinates *trans* to equivalent ligands in the structures of $[Fe_2(\mu\text{-}O_2)L^1{}_2(\mu\text{-}O_2CCH_2Ph)_2]$ and $[Fe_2(\mu\text{-}O_2)L^2(OPPh_3)_2]^{3+}$ and thus acts as a symmetric bridge between two essentially equivalent iron centers in both complexes. In contrast, the peroxide in $[Fe_2(\mu\text{-}O_2)L^3(O_2CPh)]^{2+}$ co-ordinates *trans* to an imidazole on one iron and *trans* to an amine on the other iron, resulting in distinct iron sites with Fe–O_{peroxo} bonds that differ by almost 0.1 Å in length.

A comparison of the Raman and Mössbauer properties of these synthetic dioxygen adducts with those of MMO intermediate **P** (Table 1) allows a structure for **P** to be proposed. All three synthetic adducts exhibit a resonance-enhanced Raman feature near 900 cm^{-1},[18,19,23] which downshifts by the expected 40–50 cm^{-1} upon substitution with $^{18}O_2$. Since **P** also exhibits a Raman band at 905 cm^{-1}, it is postulated to have a 1,2-peroxo bridge, like the synthetic adducts. This idea is consistent with the co-ordinative unsaturation of both iron sites in $MMOH_{red}$ and the fact that only one Mössbauer doublet is observed for **P**. However the ^{18}O shift observed for **P** is only half as large as those found for the synthetic adducts, and this smaller than expected downshift is currently not understood.

At the time of its characterization, **P** exhibited an unprecedented Mössbauer isomer shift of 0.66 mm s^{-1},[16a] about 0.1 mm s^{-1} higher than typical of a high-spin iron(III) site. Such an isomer shift value has now been observed for both iron sites of $[Fe_2(\mu\text{-}O_2)L^1{}_2(\mu\text{-}O_2CCH_2Ph)_2]$ and one iron site in $[Fe_2(\mu\text{-}O_2)L^3(O_2CPh)]^{2+}$, suggesting that the unusual isomer shift value

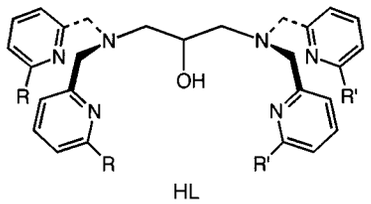

HL

R = R' = H	irreversible, observable only at ≤ -60 °C and in the presence of Ph_3PO or dmso
R = H, R' = Me	irreversible, observable at ≤ -60 °C but does not require Ph_3PO or dmso
R = R' = Me	reversible at -40 °C

Fig. 3 Comparison of the reactivities of $[Fe^{II}_2L(O_2CPh)]^{2+}$ complexes

may be associated with iron sites that can bind O_2 (Table 1). However this suggestion must be tempered by the fact that oxyhemerythrin and $[Fe_2(\mu\text{-}O_2)L^2(O_2CPh)]^{2+}$ exhibit isomer shifts typical of high-spin iron(III) centers. So the chemical significance of the unusual isomer shift is not yet understood. Nevertheless the excellent match in the properties of **P** and $[Fe_2(\mu\text{-}O_2)L^1_2(\mu\text{-}O_2CCH_2Ph)_2]$ suggests that a (μ-1,2-peroxo)-bis(μ-carboxylato)diiron(III) core structure is a good working model for **P**.

The availability of these synthetic dioxygen adducts also provides us with insight into how dioxygen binding and activation at non-heme diiron active sites may be controlled. There are at least three lessons that can be derived from these studies: (a) that co-ordinatively unsaturated metal centers are required to facilitate dioxygen binding, (b) that steric bulk and/or hydrophobicity promote reversibility and (c) that adduct stability can be modulated by ligand electronic effects.

Co-ordinative unsaturation of the metal centers involved in dioxygen binding is an important feature of oxygen binding sites in biology and is borne out by an examination of the diiron(II) active sites of the non-heme diiron proteins (Fig. 1). The earlier modeling work on these proteins afforded complexes such as $[Fe_2(\mu\text{-}OH)(O_2CMe)_2(tmtacn)_2]X$ (modeling the deoxyhemerythrin core; tmtacn = 1,4,7-trimethyl-1,4,7-triazacyclononane),[25] $[Fe_2L^4(O_2CH)_4]$ [modeling the $MMOH_{red}$ core; L^4 = bis(1-methylimidazol-2-yl)phenylmethoxymethane],[26] and $[Fe_2(tpa)_2(O_2CMe)_2][BPh_4]_2$ [modeling the $R2_{red}$ core; tpa = tris(2-pyridylmethyl)amine],[27] all of which involved co-ordinatively saturated metal centers. While these three complexes all react with O_2 to yield diiron(III) products, no transient oxygenated intermediates could be detected, even at low temperature. In contrast, the synthetic diiron(II) precursors that afford dioxygen adducts are all five-co-ordinate. In my view, the availability of a co-ordination site on each iron(II) center greatly enhances the rate of formation of the adduct, thereby allowing the intermediate to be observed and characterized.

Steric factors appear to play an important role in the formation and stability of the dioxygen adduct. In the L^1 series of complexes an adduct is not observed when a carboxylate with a tertiary alkyl group such as *tert*-butyl or adamantyl is used.[23b] An examination of the crystal structure of the precursor complex suggests that the putative dioxygen binding site is too hindered by the isopropyl groups and the bulky carboxylate to allow O_2 access to the site. With carboxylates having primary or secondary alkyl groups an adduct can form. As illustrated by the structure of $[Fe_2(\mu\text{-}O_2)L^1_2(\mu\text{-}O_2CCH_2Ph)_2]$,[20] the resulting peroxo moiety is then well shielded from the solvent by the isopropyl groups of the ligand L^1, thereby inhibiting potential bimolecular pathways for decomposition.[28]

The $[Fe_2L(O_2CPh)]^{2+}$ series of complexes (Fig. 3)[18b,19] illustrate the dramatic effects of introducing a methyl substituent at a key position. Suzuki and co-workers[19] found that the dioxygen adduct of $[Fe_2L(O_2CPh)]^{2+}$ (R = R′ = H) was not stable enough to be observed even at −80 °C. However the introduction of 6-methyl substituents on the pendant pyridines lengthened the lifetime of the corresponding adducts. When two 6-methyl substituents were introduced, an irreversible dioxygen adduct formed at −60 °C. When four 6-methyl substituents were introduced the adduct formed and binding was reversible. Thus a small change in the ligand structure gave rise to a considerable range of dioxygen adduct stabilities.

While it is tempting to attribute the differences observed in the $[Fe_2L(O_2CPh)]^{2+}$ series solely to the physical effect of the 6-methyl substituents in isolating the bound peroxide from the solvent environment, there appears also to be an electronic effect. The reversibility of dioxygen binding is controlled by the relative stabilities of the precursor and the adduct complexes. If the iron(III) state were overwhelmingly favored over the iron(II) state, then binding would be irreversible. However, if the iron(III) state can be destabilized reversible dioxygen binding may be achieved. From crystallographic comparisons, it is clear that a 6-methylpyridine ligand makes a longer $Fe–N_{py}$ bond than a pyridine, due to steric interactions of the methyl group with the metal center.[19b,29] Such a bond lengthening would favor the iron(II) over the iron(III) state based on a consideration of ionic radii. Thus the irreversible dioxygen binding found for $[Fe_2L(O_2CPh)]^{2+}$ (R = R′ = H) becomes reversible in $[Fe_2L(O_2CPh)]^{2+}$ (R = R′ = Me) as Fe^{III} becomes destabilized relative to Fe^{II}.

This notion is also emphasized in the crystal structure of $[Fe_2(\mu\text{-}O_2)L^3(O_2CPh)]^{2+}$ where the steric effects of the phenyl groups on the pendant imidazoles cause the $Fe–N_{imidazole}$ bonds to lengthen.[22] The average Fe–N bond length observed in this structure (2.16 Å) is significantly longer than that of either the iron(III) site (2.10 Å) or the iron(II) site (2.12 Å) of $[Fe_2L^5(O_2CPh)_2]^{2+}$, a related complex without the phenyl groups. The phenyl groups allow the diiron(II) complex and the dioxygen adduct to achieve a thermodynamic balance so that reversible dioxygen binding is achieved.

That electronic factors affect the stability of the dioxygen adducts is further illustrated by studies involving substitutions of the carboxylate bridge. Suzuki and co-workers[19b] found that replacement of the benzoate bridge in $[Fe_2(\mu\text{-}O_2)L(O_2CPh)]^{2+}$ (R = R′ = Me) with trifluoroacetate afforded a thermally more stable dioxygen adduct. Que and co-workers[21] monitored the decomposition of a series of $[Fe_2(\mu\text{-}O_2)L^2(O_2CC_6H_4X)]^{2+}$ adducts as a function of the phenyl ring substituent X and found the rate of decomposition † at −10 °C to correlate with σ, affording a ρ value of −1.1.[21] These observations indicate that the stability of the (μ-1,2-peroxo)diiron(III) unit can be modulated by the amount of electron donation by the ligands, with increasing electron density required to activate the O–O bond. This correlation rationalizes the effect of Ph_3PO or dimethyl sulfoxide (dmso) on the dioxygen adducts of $[Fe_2L(O_2CPh)]^{2+}$ (R = R′ = H).[18] In the crystal structure of $[Fe_2(\mu\text{-}O_2)L^2(OPPh_3)_2]^{3+}$ the anionic carboxylate bridge has been replaced by neutral phosphine oxide ligands, thereby decreasing the electron density at the diiron center and stabilizing the dioxygen adduct.[21] When extended to the non-heme diiron proteins, this correlation can be used to rationalize the use of a histidine-rich diiron center for a reversible dioxygen-binding protein such as hemerythrin and a carboxylate-rich diiron center for dioxygen-activating enzymes such as RNR R2, MMOH, and Δ9D.

High-valent Intermediates after O–O Bond Cleavage

High-valent intermediates have been observed in the oxidative reaction cycles of MMOH and RNR R2.[14–16] For MMOH, intermediate **P** converts into **Q**, the species responsible for the hydroxylation of methane;[15,16] MMOH-**Q** is assigned as an anti-

† There is disagreement about the decomposition mechanism of the adduct which remains to be resolved. Dong *et al.*[21] observed a first-order decomposition process, while Feig *et al.*[28] found a second-order decomposition process.

Table 2 Properties of high-valent diiron species

Complex	Spin state	d(Fe···Fe)/Å	δ/mm s^{-1}	Ref.
RNR R2-**X**	$\frac{1}{2}$		0.26, 0.50	33(*b*)
MMOH-**Q** (*Methylosinus trichosporium*)	0	2.46 (EXAFS)	0.17	15(*b*), 34
MMOH-**Q** (*Methylococcus capsulatus*)	0		0.14, 0.21	16(*a*)
$[Fe_2(\mu\text{-}O)_2(tpa)_2]^{3+}$	$\frac{3}{2}$		0.11	30
$[Fe_2(\mu\text{-}O)_2(5\text{-}Me_3\text{-}tpa)_2]^{3+}$	$\frac{3}{2}$	2.89 (EXAFS)	0.14	24
$[Fe_2(\mu\text{-}O)_2(6\text{-}Me\text{-}tpa)_2]^{3+}$	$\frac{1}{2}$		0.08, 0.48	31
$[Fe_2(\mu\text{-}O)_2(6\text{-}Me_3\text{-}tpa)_2]^{2+}$	0	2.71 (X-ray)	0.50	32

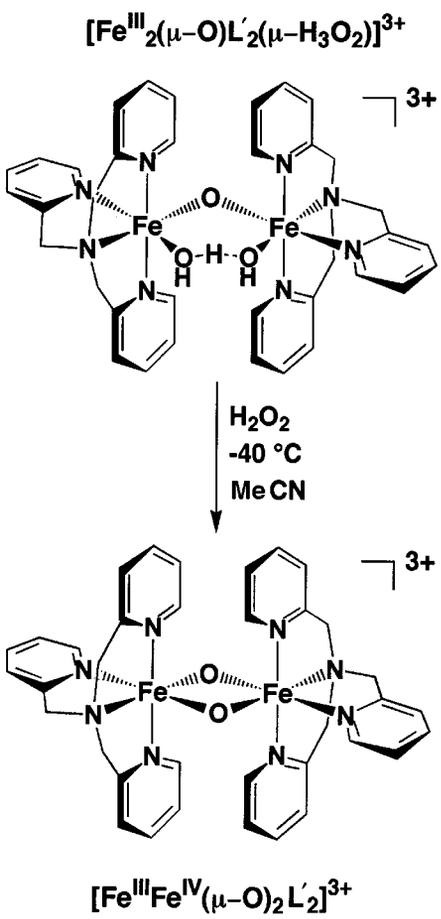

Scheme 2 General reaction for the formation of the $[Fe_2(\mu\text{-}O)_2]^{3+}$ diamond core

ferromagnetically coupled diiron(IV) species on the basis of its Mössbauer properties (Table 2). For RNR R2, intermediate **X**, probably formed upon one-electron reduction of a '**P**-like' species, generates the tyrosyl 122 radical, which is catalytically essential for the deoxygenation of ribonucleotides.[14] The species RNR R2-**X** is formally an iron(III)iron(IV) complex and exhibits an isotropic EPR signal at $g = 2$ arising from its $S = \frac{1}{2}$ ground state (Table 2). There has been extensive discussion about its precise electronic description, some of which will be summarized in a later section.

Analogous high-valent species have not been observed from the decomposition of the synthetic diiron dioxygen adducts described in the previous section. Only one of these, $[Fe_2(\mu\text{-}O_2)L(OPPh_3)_2]^{3+}$ (R = R′ = H), has been found to oxidize a substrate related to those of the enzymes of interest, *i.e.* 2,4-di-*tert*-butylphenol which is analogous to Tyr-122 of RNR R2,[18*b*] but none of these has been reported to effect hydrocarbon oxidation thus far. This lack of reactivity may derive from the restrictions imposed by the ligand design to stabilize the dioxygen adducts. Such constraints either prevent access to the desired higher-valent species or shorten the lifetime of any high-valent species that may be formed in the decomposition of these (μ-1,2-peroxo)diiron(III) complexes by precluding drastic changes in core structure that may be necessary to achieve the next higher oxidation state.

Que and co-workers have found the only synthetic system thus far to yield high-valent complexes by reaction of a diiron complex with a dioxygen species. As precursors, they used sterically less demanding (μ-oxo)diiron(III) complexes supported by the readily displaceable $H_3O_2^-$ bridge, $[Fe^{III}_2(\mu\text{-}O)L'_2(\mu\text{-}H_3O_2)]^{3+}$ (L′ = tpa and its ring-alkylated derivatives). Treatment of these diiron(III) complexes with H_2O_2 affords $[Fe^{III}Fe^{IV}(\mu\text{-}O)_2L'_2]^{3+}$ (Scheme 2) by a mechanism yet to be elucidated.[24,30,31] Unfortunately, the instability of the complexes has thus far prevented crystallographic characterization, but the lifetime of the complex can be extended by lowering the temperature to −40 °C and/or introducing alkyl substituents in the 5 position of the pyridine rings, thereby allowing a number of spectroscopic experiments to be carried out.

The molecular composition of the high-valent species was determined by electrospray ionization mass spectrometry. The mass spectrum of $[Fe_2(\mu\text{-}O)_2(5\text{-}Me_3\text{-}tpa)_2][ClO_4]_3$ [5-Me$_3$-tpa = tris(5-methyl-2-pyridylmethyl)amine] showed positive and negative ions with *m*/*z* values consistent with the formulae $\{[Fe_2(\mu\text{-}O)_2(5\text{-}Me_3\text{-}tpa)_2][ClO_4]_2\}^+$ and $\{[Fe_2(\mu\text{-}O)_2(5\text{-}Me_3\text{-}tpa)_2][ClO_4]_4\}^-$, respectively [Fig. 4(*a*)].[24] In addition, because of the differing number of perchlorates, the two ions gave rise to distinctive isotope distribution patterns that allowed the number of chlorine atoms in the ion to be counted and provide unequivocal support for the elemental composition of the complex. Similar mass spectral information was obtained for $[Fe_2(\mu\text{-}O)_2(6\text{-}Me\text{-}tpa)][ClO_4]_3$ [6-Me-tpa = (6-methyl-2-pyridylmethyl)bis(2-pyridylmethyl)amine].[31]

Since mass spectrometry can only provide information on the molecular composition, the structure of $[Fe_2(\mu\text{-}O)_2(5\text{-}Me_3\text{-}tpa)_2][ClO_4]_3$ was deduced from EXAFS studies.[24] Its Fourier-transformed EXAFS spectrum revealed the presence of an intense feature in the 2.5–3.0 Å range [Fig. 4(*b*)] that was fitted by an iron scatterer at 2.89 Å. Such intense second-shell features are commonly found in the EXAFS spectra of complexes with $M_2(\mu\text{-}O)_2$ diamond cores,[35] which are quite common in manganese chemistry.[36] This feature has served as the EXAFS signature for the diamond core in the active sites of super-oxidized manganese catalase[37] and the oxygen-evolving complex in photosynthesis.[35] The intense 2.89 Å feature in the spectrum of $[Fe_2(\mu\text{-}O)_2(5\text{-}Me_3\text{-}tpa)_2][ClO_4]_3$, taken together with the mass spectral data, thus strongly implicates a structure with an $Fe_2(\mu\text{-}O)_2$ diamond core (Fig. 5).

The only crystallographically characterized complex with an $Fe_2(\mu\text{-}O)_2$ diamond core is $[Fe^{III}_2(\mu\text{-}O)_2(6\text{-}Me_3\text{-}tpa)_2][ClO_4]_2$ [6-Me$_3$-tpa = tris-(6-methyl-2-pyridylmethyl)amine],[32] and its core dimensions are compared with those of $[Fe^{III}Fe^{IV}(\mu\text{-}O)_2(5\text{-}Me_3\text{-}tpa)_2][ClO_4]_3$ in Fig. 5. The Fe···Fe separation is 2.71 Å, as found for $Mn_2(\mu\text{-}O)_2$ complexes. However, the Fe–μ-O bonds are longer than any other Fe–μ-O bonds found in a (μ-oxo)diiron complex,[38] which is most likely due to the constraints associated with the formation of the $Fe_2(\mu\text{-}O)_2$ diamond core. Furthermore there is a significant bond-length asymmetry in the Fe–O–Fe unit ($\Delta r_{Fe-O} = 0.08$ Å), which is not found in the cores of related $Mn_2(\mu\text{-}O)_2$[36] and $Cu_2(\mu\text{-}O)_2$ com-

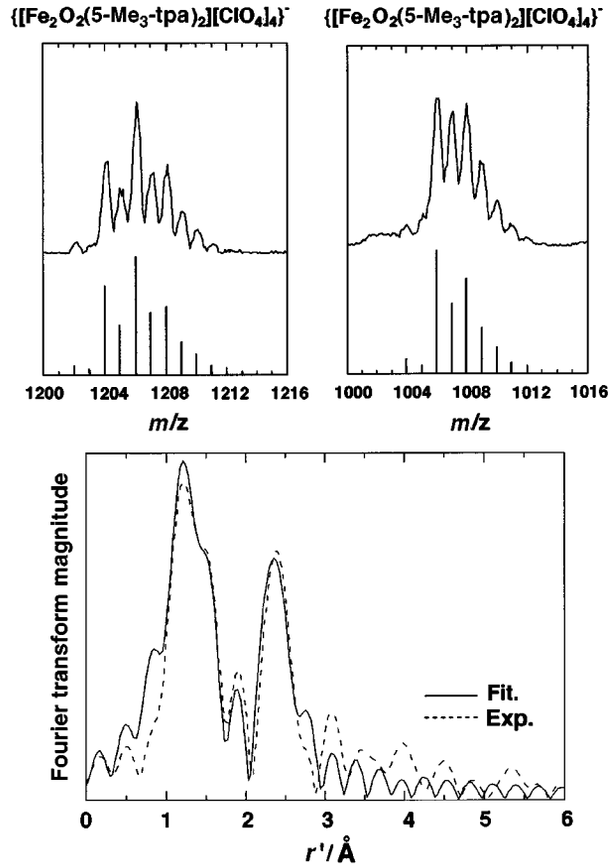

Fig. 4 Upper panel: electrospray ionization mass spectra of $[Fe_2(\mu\text{-}O)_2(5\text{-}Me_3\text{-}tpa)_2][ClO_4]_3$. Lower panel: Fourier-transformed extended X-ray absorption fine structure (EXAFS) data ($k = 2$–13 Å^{-1}) of $[Fe_2(\mu\text{-}O)_2(5\text{-}Me_3\text{-}tpa)_2][ClO_4]_3$. Reproduced with permission from the publishers of ref. 24

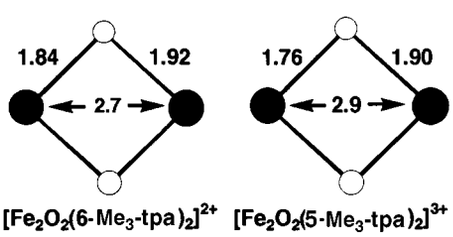

Fig. 5 Core structures (distances in Å) of $[Fe_2(\mu\text{-}O)_2(6\text{-}Me_3\text{-}tpa)_2][ClO_4]_2$ derived from X-ray crystallography (left) and $[Fe_3(\mu\text{-}O)_2(5\text{-}Me_3\text{-}tpa)_2][ClO_4]_3$ derived from EXAFS analysis (right)

plexes.[39] This core asymmetry appears also to be present in $[Fe^{III}Fe^{IV}(\mu\text{-}O)_2(5\text{-}Me_3\text{-}tpa)_2][ClO_4]_3$ as deduced by EXAFS[24] and may be characteristic of the $Fe_2(\mu\text{-}O)_2$ core. More examples are needed to uncover the rationale for this core asymmetry.

Two types of $[Fe^{III}Fe^{IV}(\mu\text{-}O)_2L_2][ClO_4]_3$ complexes have been characterized thus far. An $S = \frac{3}{2}$ species is obtained for L = tpa or a 5-alkylated derivative,[24] while an $S = \frac{1}{2}$ species is formed when L = 6-Me-tpa.[31] The different electronic properties can be understood by considering the spin states of the iron ions in the two types of complexes (Fig. 6). The $S = \frac{1}{2}$ species derives from antiferromagnetically coupled high-spin Fe^{III} ($S_1 = \frac{5}{2}$) and high-spin Fe^{IV} ($S_2 = 2$) ions, consistent with the observation of two Mössbauer doublets having isomer shifts that correspond to the two different oxidation states [$\delta = 0.48$ mm s^{-1} for the iron(III) site and 0.08 mm s^{-1} for the iron(IV) site]. On the other hand, the $S = \frac{3}{2}$ species is a valence-delocalized pair consisting of a low-spin iron(III) ($S_1 = \frac{1}{2}$) ion and a low-spin iron(IV) ($S_2 = 1$) ion, as indicated by the observation of only one doublet in its Mössbauer spectrum ($\delta = 0.14$ mm s^{-1}). The change in spin state from low to high upon the introduction of a 6-methyl group can be understood by the same principles applied to the reversibility

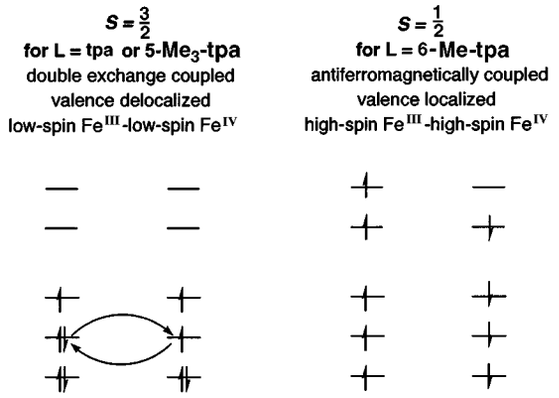

Fig. 6 Spin-coupling schemes rationalizing the $S = \frac{3}{2}$ ground state of $[Fe_2(\mu\text{-}O)_2(5\text{-}Me_3\text{-}tpa)_2]^{3+}$ and the $S = \frac{1}{2}$ ground state of $[Fe_2(\mu\text{-}O)_2(6\text{-}Me\text{-}tpa)_2]^{3+}$

of dioxygen binding discussed in the preceding section; in this context, the presence of the 6-methyl substituent strongly disfavors ions of smaller ionic radius (*i.e.* low-spin Fe).[29]

How do these synthetic complexes relate to the high-valent species found in the non-heme diiron enzymes? Since the diiron active sites are all carboxylate-rich, it is unlikely that the iron ions will have low-spin configurations. Thus the only model for spectroscopic comparison with high-valent enzyme intermediates is $[Fe_2(\mu\text{-}O)_2(6\text{-}Me\text{-}tpa)_2]^{3+}$. The species RNR R2-**X** shares the same formal $Fe^{III}Fe^{IV}$ oxidation level as the model, and both have $S = \frac{1}{2}$ ground spin states. Initial analysis of the spectroscopic properties of RNR R2-**X** led the investigators to disfavor an $Fe^{III}Fe^{IV}$ description for the intermediate.[14d] The isotropic EPR signal at $g = 2$ observed for RNR R2-**X** appeared inconsistent with the presence of an anisotropic high-spin iron(IV) ion; instead a description involving two iron(III) ions and a ligand radical was favored. Two subsequent observations led to a reconsideration which now favors the $Fe^{III}Fe^{IV}$ model: (a) the finding that $[Fe_2(\mu\text{-}O)_2(6\text{-}Me\text{-}tpa)_2]^{3+}$ also exhibited an isotropic $g = 2$ signal, despite having an anisotropic high-spin iron(IV) ion,[31] and (b) electron nuclear double resonance (ENDOR) data on RNR R2-**X** showing that one of the iron ions was indeed anisotropic.[33] However the properties of RNR R2-**X** and $[Fe_2(\mu\text{-}O)_2(6\text{-}Me\text{-}tpa)_2]^{3+}$ are not identical. The 'iron(IV)' site in RNR R2-**X** has an isomer shift 0.2 mm s^{-1} more positive than that for the model (0.26 *vs.* 0.08 mm s^{-1}) and a smaller anisotropy ($\Delta a = 7.0$ *vs.* 12.4 MHz). These differences may arise from variations in metal–ligand covalency due to the nature of terminal ligands and/or distinct core structures. The lack of a sufficient database of well characterized iron(IV) complexes hampers interpretation of these spectroscopic differences.

The diiron(IV) intermediate MMOH-**Q** does not have a synthetic analogue at present, but insight into its core structure has recently been obtained from tandem rapid freeze–quench Mössbauer/EXAFS experiments.[34] These show that MMOH-**Q** has an Fe···Fe distance of 2.5 Å and one short 1.8 Å Fe–O bond per Fe, in addition to four metal–ligand bonds that average 2.04 Å. Precedents from model compounds indicate that, to achieve the short metal–metal distance, the diiron(IV) unit must have three bridges with at least two being monoatomic. The typical Mn···Mn distance of 2.7 Å in complexes with bis-(μ-oxo) cores is shortened to *ca.* 2.6 Å upon addition of a bidentate carboxylate bridge;[40] thus an analogous core structure may be considered for MMOH-**Q** [Fig. 7(*a*)]. Alternatively, a structure with three single-atom bridges [Fig. 7(*b*)] can also exhibit such a short distance, as found for $[Fe_2(\mu\text{-}OH)_3(tmtacn)_2]^{2+}$ (2.5 Å[41]) and $[Mn_2(\mu\text{-}O)_3(tmtacn)_2]^{2+}$ (2.3 Å[40]). Since the $Fe_2(\mu\text{-}O)_2$ diamond core has been demonstrated to support the iron(IV) oxidation state in a non-heme ligand environment, this core structure is favored for MMOH-**Q** at present. In this model, the $Fe_2(\mu\text{-}O)_2$ core would exhibit a core

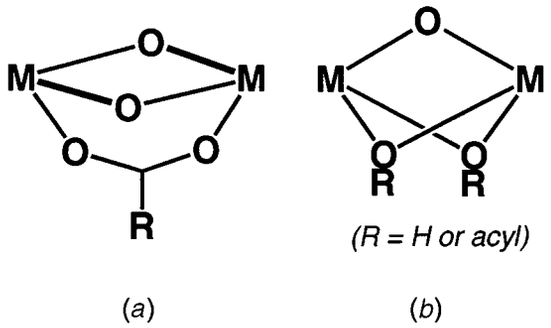

(*a*) (*b*)

Fig. 7 Possible-core structures of MMOH-**Q**

asymmetry like that found for $[Fe_2(\mu\text{-}O)_2(6\text{-}Me_3\text{-}tpa)_2]^{2+}$ and $[Fe_2(\mu\text{-}O)_2(5\text{-}Me_3\text{-}tpa)_2]^{3+}$ to be consistent with the single short Fe–O bond per iron. Completely independent density functional theory calculations also favor this core structure for MMOH-**Q**, and core dimensions closely matching the experimentally obtained values were obtained.[42]

Given the correspondence in spectroscopic properties between the high-valent enzyme intermediates and the synthetic $Fe_2(\mu\text{-}O)_2$ complexes, it would also be useful to compare their reactivities. Owing to their metastable and high-valent nature, it seems likely that the synthetic complexes could serve as oxidizing agents. Thus far, detailed reactivity information is available only for $[Fe_2(\mu\text{-}O)_2(tpa)_2]^{3+}$. This complex can oxidize substrates related to those oxidized by the diiron centers of RNR, MMO and Δ9D.[43] It quantitatively oxidizes 2,4-di-*tert*-butylphenol to its phenoxy radical within seconds at −40 °C and is reduced to its (μ-oxo)diiron(III) precursor, equation (1).

$$[Fe_2(\mu\text{-}O)_2(tpa)_2]^{3+} + PhOH \longrightarrow [Fe_2(\mu\text{-}O)(\mu\text{-}OH)(tpa)_2]^{3+} + PhO^{\bullet} \quad (1)$$

This reaction thus models the oxidation of Tyr-122 by RNR-R2 **X** in the assembly of the diiron(III)–tyrosyl radical cofactor found in active RNR R2.[14]

The complex $[Fe_2(\mu\text{-}O)_2(tpa)_2]^{3+}$ also oxidizes cumene and affords $PhC(OH)Me_2$ and α-methylstyrene in excellent yield (88%).[43] The observed products respectively derive from hydroxylation and desaturation of the substrate, analogous to reactions catalysed by MMO and fatty acid desaturases. Since $[Fe_2(\mu\text{-}O)_2(tpa)_2]^{3+}$ is only a one-electron oxidant, 2 equivalents are required per product molecule formed, and substrate oxidation must occur in two steps, *i.e.* equations (2) and (3). The

$$[Fe_2(\mu\text{-}O)_2(tpa)_2]^{3+} + PhCH(Me)_2 \longrightarrow [Fe_2(\mu\text{-}O)(\mu\text{-}OH)(tpa)_2]^{3+} + PhC^{\bullet}Me_2 \quad (2)$$

$$[Fe_2(\mu\text{-}O)_2(tpa)_2]^{3+} + PhC^{\bullet}(Me)_2 \longrightarrow [Fe_2(\mu\text{-}O)(tpa)_2]^{4+} + PhC(OH)Me_2 \text{ or } [Fe_2(\mu\text{-}O)(\mu\text{-}OH)(tpa)_2]^{3+} + PhC(Me){=}CH_2 \quad (3)$$

formation of an alkyl radical intermediate was demonstrated by trapping it with O_2 to afford products derived from the breakdown of the cumylperoxy radical. Furthermore, the decomposition of $[Fe_2(\mu\text{-}O)_2(tpa)_2]^{3+}$ in the presence of ethylbenzene or $[^2H_{10}]$ethylbenzene showed a kinetic isotope effect of 20 at −40 °C, consistent with rate-determining C–H bond cleavage. Similar values were obtained for the cleavage of C–H bonds by the related $[Cu_2(\mu\text{-}O)_2(R_3tacn)_2]^{2+}$ ($k_H/k_D = 26 \pm 2$ for R = Pr^i and 40 for R = benzyl at −40 °C)[44] and by MMOH-**Q** ($k_H/k_D \geqslant 20$ at 4 °C).[45] In agreement, competition experiments using a mixture of ethylbenzene and $[^2H_{10}]$ethylbenzene yielded product ratios of 22 ± 3 : 1 for protio- and deuterio-alcohol and 28 ± 3 : 1 for protio- and deuterio-styrene. These results demonstrate that cleavage of the substrate α-C–H bond is a major component of the rate-determining step for both hydroxylation and desaturation. Moreover the significantly smaller isotope effect (*ca.* 1.3, estimated from 28/22) for the cleavage of the β-C–H bond to form styrene indicates that desaturation must involve asynchronous scission of the two C–H bonds, as has been observed for yeast Δ9D.[46] Thus, despite its somewhat limited oxidizing power (no reaction with cyclohexane, for example), $[Fe_2(\mu\text{-}O)_2(tpa)_2]^{3+}$ displays a versatile oxidative reactivity that encompasses the range of reactions catalyzed by the non-heme diiron enzymes. This versatility supports the notion illustrated in Scheme 1 that a high-valent species with an $Fe_2(\mu\text{-}O)_2$ diamond core (or some variations thereof) may be the common feature of the oxidative mechanisms of this family of enzymes.

In conclusion, the past few years have seen significant developments in our understanding of how a non-heme diiron active site can participate in oxygen-activation chemistry. However a number of important challenges still remain; these include determining: (a) how a diiron–peroxo species is converted into a high-valent intermediate, (b) what types of core structures are required to stabilize high oxidation states, and (c) how such high-valent species react with organic substrates. As illustrated in this perspective, biomimetic approaches can play a key role in uncovering details of the reaction mechanism and, in particular, provide precedents for possible structures for the intermediates involved in this chemistry.

Acknowledgements

The studies from my laboratory discussed in this perspective were supported by the National Institutes of Health (GM-38767) and the National Science Foundation (MCB-9405723).

References

1 (*a*) B. J. Wallar and J. D. Lipscomb, *Chem. Rev.*, 1996, **96**, 2625; (*b*) A. L. Feig and S. J. Lippard, *Chem. Rev.*, 1994, **94**, 759; (*c*) L. Que, jun. and A. E. True, *Prog. Inorg. Chem.*, 1990, **38**, 97.
2 R. E. Stenkamp, *Chem. Rev.*, 1994, **94**, 715.
3 (*a*) P. Nordlund and H. Eklund, *J. Mol. Biol.*, 1993, **232**, 123; (*b*) D. T. Logan, X.-D. Su, A. Åberg, K. Regnström, J. Hajdu, H. Eklund and P. Nordlund, *Struct. Bonding* (*Berlin*), 1996, **4**, 1053.
4 (*a*) A. C. Rosenzweig, C. A. Frederick, S. J. Lippard and P. Nordlund, *Nature* (*London*), 1993, **366**, 537; (*b*) A. C. Rosenzweig, P. Nordlund, P. M. Takahara, C. A. Frederick and S. J. Lippard, *Chem. Biol.*, 1995, **2**, 409; (*c*) N. Elango, R. Radhakrishnam, W. A. Froland, B. J. Wallar, C. A. Earhart, J. D. Lipscomb and D. H. Ohlendorf, *Protein Sci.*, 1997, **6**, 556.
5 Y. Lindqvist, W. Huang, G. Schneider and J. Shanklin, *EMBO J.*, 1996, **15**, 4081.
6 (*a*) S. J. Lippard and J. M. Berg, *Principles of Bioinorganic Chemistry*, University Science Books, Mill Valley, CA, 1994; (*b*) L. Que, jun., in *Bioinorganic Catalysis*, ed. J. Reedijk, Marcel Dekker, New York, 1993, pp. 347–393.
7 (*a*) P. Nordlund, H. Dalton and H. Eklund, *FEBS Lett.*, 1992, **307**, 257; (*b*) B. G. Fox, J. Shanklin, J. Ai, T. M. Loehr and J.-S. Loehr, *Biochemistry*, 1994, **33**, 12 776.
8 A. K. Shiemke, T. M. Loehr and J. Sanders-Loehr, *J. Am. Chem. Soc.*, 1986, **108**, 2437.
9 J. D. Pikus, J. M. Studts, C. Achim, K. E. Kauffmann, E. Münck, R. J. Steffan, K. McClay and B. G. Fox, *Biochemistry*, 1996, **35**, 9106.
10 B. G. Fox, J. Shanklin, C. Somerville and E. Münck, *Proc. Natl. Acad. Sci. USA*, 1993, **90**, 2486; J. Ai, J. A. Broadwater, T. M. Loehr, J. Sanders-Loehr and B. G. Fox, *J. Biol. Inorg. Chem.*, 1997, **2**, 37.
11 R. L. Rardin, W. B. Tolman and S. J. Lippard, *New J. Chem.*, 1991, **15**, 417.
12 L. Que, jun., *Science*, 1991, **253**, 273; L. Que, jun. and Y. Dong, *Acc. Chem. Res.*, 1996, **29**, 190.
13 D. E. Edmondson and B.-H. Huynh, *Inorg. Chim. Acta*, 1996, **252**, 399; A. A. Shteinman, *FEBS Lett.*, 1995, **362**, 5.
14 (*a*) J. M. Bollinger, jun., D. E. Edmondson, B. H. Huynh, J. Filley, J. Norton and J. Stubbe, *Science* (*Washington, DC*), 1991, **253**, 292; (*b*) J. M. Bollinger, jun., W. H. Tong, N. Ravi, B. H. Huynh, D. E. Edmondson and J. Stubbe, *J. Am. Chem. Soc.*, 1994, **116**, 8015; (*c*) J. M. Bollinger, jun., W. H. Tong, N. Ravi, B. H. Huynh, D. E. Edmondson and J. Stubbe, *J. Am. Chem. Soc.*, 1994, **116**, 8024;

(*d*) N. Ravi, J. J. M. Bollinger, B. H. Huynh, D. E. Edmondson and J. Stubbe, *J. Am. Chem. Soc*., 1994, **116**, 8007; (*e*) W. H. Tong, S. Chen, S. G. Lloyd, D. E. Edmondson, B. H. Huynh and J. Stubbe, *J. Am. Chem. Soc*., 1996, **118**, 2107.
15 (*a*) S.-K. Lee, J. C. Nesheim and J. D. Lipscomb, *J. Biol. Chem*., 1993, **268**, 21 569; (*b*) S.-K. Lee, B. G. Fox, W. A. Froland, J. D. Lipscomb and E. Münck, *J. Am. Chem. Soc*., 1993, **115**, 6450.
16 (*a*) K. E. Liu, D. Wang, B. H. Huynh, D. E. Edmondson, A. Salifoglou and S. J. Lippard, *J. Am. Chem. Soc*., 1994, **116**, 7465; (*b*) K. E. Liu, A. M. Valentine, D. Qiu, D. E. Edmondson, E. H. Appelman, T. G. Spiro and S. J. Lippard, *J. Am. Chem. Soc*., 1995, **117**, 4997.
17 M. Y. Okamura, I. M. Klotz, C. E. Johnson, M. R. C. Winter and R. J. P. Williams, *Biochemistry*, 1969, **8**, 1951; P. E. Clark and J. Webb, *Biochemistry*, 1981, **20**, 4628.
18 (*a*) S. Ménage, B. A. Brennan, C. Juarez-Garcia, E. Münck and L. Que, jun., *J. Am. Chem. Soc*., 1990, **112**, 6423; (*b*) Y. Dong, S. Ménage, B. A. Brennan, T. E. Elgren, H. G. Jang, L. L. Pearce and L. Que, jun., *J. Am. Chem. Soc*., 1993, **115**, 1851.
19 (*a*) Y. Hayashi, M. Suzuki, A. Uehara, Y. Mizutani and T. Kitagawa, *Chem. Lett*., 1992, 91; (*b*) Y. Hayashi, T. Kayatani, H. Sugimoto, M. Suzuki, K. Inomata, A. Uehara, Y. Mizutani, T. Kitagawa and Y. Maeda, *J. Am. Chem. Soc*., 1995, **117**, 11 220.
20 K. Kim and S. J. Lippard, *J. Am. Chem. Soc*., 1996, **118**, 4914.
21 Y. Dong, S. Yan, V. G. Young, jun. and L. Que, jun., *Angew. Chem.*, *Int. Ed. Engl*., 1996, **35**, 618.
22 T. Ookubo, H. Sugimoto, T. Nagayama, H. Masuda, T. Sato, K. Tanaka, Y. Maeda, H. Okawa, Y. Hayashi, A. Uehara and M. Suzuki, *J. Am. Chem. Soc*., 1996, **118**, 701.
23 (*a*) N. Kitajima, H. Fukui, Y. Moro-oka, Y. Mizutani and T. Kitagawa, *J. Am. Chem. Soc*., 1990, **112**, 6402; (*b*) N. Kitajima, N. Tamura, H. Amagai, H. Fukui, Y. Moro-oka, Y. Mizutani, T. Kitagawa, R. Mathur, K. Heerwegh, C. A. Reed, C. R. Randall, L. Que, jun. and K. Tatsumi, *J. Am. Chem. Soc*., 1994, **116**, 9071.
24 Y. Dong, H. Fujii, M. P. Hendrich, R. A. Leising, G. Pan, C. R. Randall, E. C. Wilkinson, Y. Zang, L. Que, jun., B. G. Fox, K. Kauffmann and E. Münck, *J. Am. Chem. Soc*., 1995, **117**, 2778.
25 P. Chaudhuri, K. Wieghardt, B. Nuber and J. Weiss, *Angew. Chem*., *Int. Ed. Engl*., 1985, **24**, 778; J. R. Hartman, R. L. Rardin, P. Chaudhuri, K. Pohl, K. Wieghardt, B. Nuber, J. Weiss, G. C. Papaefthymiou, R. B. Frankel and S. J. Lippard, *J. Am. Chem. Soc*., 1987, **109**, 7387.
26 W. B. Tolman, S. Liu, J. G. Bentsen and S. J. Lippard, *J. Am. Chem. Soc*., 1991, **113**, 152.
27 S. Ménage, Y. Zang, M. P. Hendrich and L. Que, jun., *J. Am. Chem. Soc*., 1992, **114**, 7786.
28 A. L. Feig, M. Becker, S. Schindler, R. van Eldik and S. J. Lippard, *Inorg. Chem*., 1996, **35**, 2590.
29 Y. Zang, J. Kim, Y. Dong, E. C. Wilkinson, E. H. Appelman and L. Que, jun., *J. Am. Chem. Soc*., 1997, **119**, 4197.
30 R. A. Leising, B. A. Brennan, L. Que, jun., B. G. Fox and E. Münck, *J. Am. Chem. Soc*., 1991, **113**, 3988.
31 Y. Dong, L. Que, jun., K. Kauffmann and E. Münck, *J. Am. Chem. Soc*., 1995, **117**, 11 377.
32 Y. Zang, Y. Dong, L. Que, jun., K. Kauffmann and E. Münck, *J. Am. Chem. Soc*., 1995, **117**, 1169.
33 (*a*) D. Burdi, B. E. Sturgeon, W. H. Tong, J. Stubbe and B. M. Hoffman, *J. Am. Chem. Soc*., 1996, **118**, 281; (*b*) B. E. Sturgeon, D. Burdi, S. Chen, B.-H. Huynh, D. E. Edmondson, J. Stubbe and B. M. Hoffman, *J. Am. Chem. Soc*., 1996, **118**, 7551.
34 L. Shu, J. C. Nesheim, K. Kauffmann, E. Münck, J. D. Lipscomb and L. Que, jun., *Science*, 1997, **275**, 515.
35 V. K. Yachandra, K. Sauer and M. P. Klein, *Chem. Rev*., 1996, **96**, 2927.
36 R. Manchanda, G. W. Brudvig and R. H. Crabtree, *Coord. Chem. Rev*., 1995, **144**, 1.
37 G. S. Waldo, S. Yu and J. E. Penner-Hahn, *J. Am. Chem. Soc*., 1992, **114**, 5869.
38 D. M. Kurtz, jun., *Chem. Rev*., 1990, **90**, 585.
39 S. Mahapatra, J. A. Halfen, E. C. Wilkinson, G. Pan, X. Wang, V. G. Young, jun., C. J. Cramer, L. Que, jun. and W. B. Tolman, *J. Am. Chem. Soc*., 1996, **118**, 11 555; S. Mahapatra, V. G. Young, jun., S. Kaderli, A. D. Zuberbühler and W. B. Tolman, *Angew. Chem*., *Int. Ed. Engl*., 1997, **36**, 130.
40 K. Wieghardt, U. Bossek, B. Nuber, J. Weiss, J. Bonvoisin, M. Corbella, S. E. Vitols and J.-J. Girerd, *J. Am. Chem. Soc*., 1988, **110**, 7398; S. Pal, J. W. Gohdes, W. C. A. Wilisch and W. H. Armstrong, *Inorg. Chem*., 1992, **31**, 713.
41 D. R. Gamelin, E. Bominaar, M. L. Kirk, K. Wieghardt and E. I. Solomon, *J. Am. Chem. Soc*., 1996, **118**, 8085; X.-Q. Ding, E. L. Bominaar, E. Bill, H. Winkler, A. X. Trautwein, S. Drüeke, P. Chaudhuri and K. Wieghardt, *J. Chem. Phys*., 1990, **92**, 178.
42 P. Siegbahn and R. H. Crabtree, *J. Am. Chem. Soc*., 1997, **119**, 3103.
43 C. Kim, Y. Dong and L. Que, jun., *J. Am. Chem. Soc*., 1997, **119**, 3635.
44 S. Mahapatra, J. A. Halfen and W. B. Tolman, *J. Am. Chem. Soc*., 1996, **118**, 11 575.
45 J. C. Nesheim and J. D. Lipscomb, *Biochemistry*, 1996, **35**, 10 240.
46 P. H. Buist and B. Behrousian, *J. Am. Chem. Soc*., 1996, **118**, 9295.

Received 14*th May* 1997; *Paper* 7/03345A